



## Imaging Cardiac Sarcoidosis, Amyloidosis, and Cardiovascular Prosthetic Infections

# 13

Sharmila Dorbala and Rodney H. Falk

Advances in cardiovascular and molecular imaging have transformed the evaluation and management of patients with infiltrative and infectious heart diseases over the past 10 years. Today, an array of tracers are available for imaging: 2-[<sup>18</sup>F]fluoro-2-deoxy-glucose (<sup>18</sup>F-FDG), a tracer of glucose metabolism to image inflammation or infection; <sup>99m</sup>technetium (<sup>99m</sup>Tc)-pyrophosphate, <sup>99m</sup>Tc-3,3-diphosphono-1,2-propanodicarboxylic acid (<sup>99m</sup>Tc-DPD), and <sup>99m</sup>Tc-hydroxy methylene diphosphonate (<sup>99m</sup>Tc-HMDP), bone imaging tracers repurposed to image cardiac transthyretin amyloidosis (ATTR); and <sup>18</sup>F-florbetapir, <sup>18</sup>F-flutemetamol, and <sup>18</sup>F-florbetaben, targeted β-amyloid tracers to image cardiac transthyretin (ATTR) and light chain amyloidosis (AL). These advanced imaging methods are now providing substantial advantages over endomyocardial biopsy, the common reference method. Widely available, non-invasive, and immune to the challenges of sampling error, imaging improves our ability to quantify disease burden and to assess response to therapy. This chapter discusses the role of radionuclide imaging in the evaluation of cardiac sarcoidosis, cardiovascular prosthetic infection, and cardiac amyloidosis.

---

S. Dorbala (✉)

Division of Nuclear Medicine, Cardiovascular Imaging Section,  
Department of Radiology and Medicine, Brigham and Women's  
Hospital, Boston, MA, USA  
e-mail: [sdorbala@bwh.harvard.edu](mailto:sdorbala@bwh.harvard.edu)

R. H. Falk

Department of Medicine, Cardiovascular Medicine, Brigham and  
Women's Hospital, Boston, MA, USA

## Cardiac Sarcoidosis

Cardiac sarcoidosis represents a major cause of mortality in patients with systemic sarcoidosis [1], a granulomatous disorder of unknown etiology characterized by focal noncaseating granulomas in the various organ systems [2]. Because of patchy involvement of the heart with sarcoid granulomas sampling error can limit the diagnostic yield of endomyocardial biopsy (Fig. 13.1).



**Fig. 13.1** Challenges of endomyocardial biopsy in cardiac sarcoidosis. Shown is a section of an explanted heart from a patient with advanced cardiac sarcoidosis who underwent cardiac transplantation. The left ventricle shows regions of normal myocardium as well as fibrosis and inflammation. A blind endomyocardial biopsy from the right side of the interventricular septum may reveal normal myocardium, nonspecific inflammation (**a**, **b**), typical noncaseating granuloma from sarcoidosis

(**c**) or myocardial fibrosis (**d**). In sarcoidosis, these pathologies may coexist in different regions of the same heart, so it is challenging to make management decisions based on random endomyocardial biopsy results. In contrast, imaging with  $^{18}\text{F}$ -FDG PET/CT offers the ability to evaluate the whole-heart and whole-body burden of inflammation. (From Dorbala and Shaw [3]; with permission from Springer Nature)

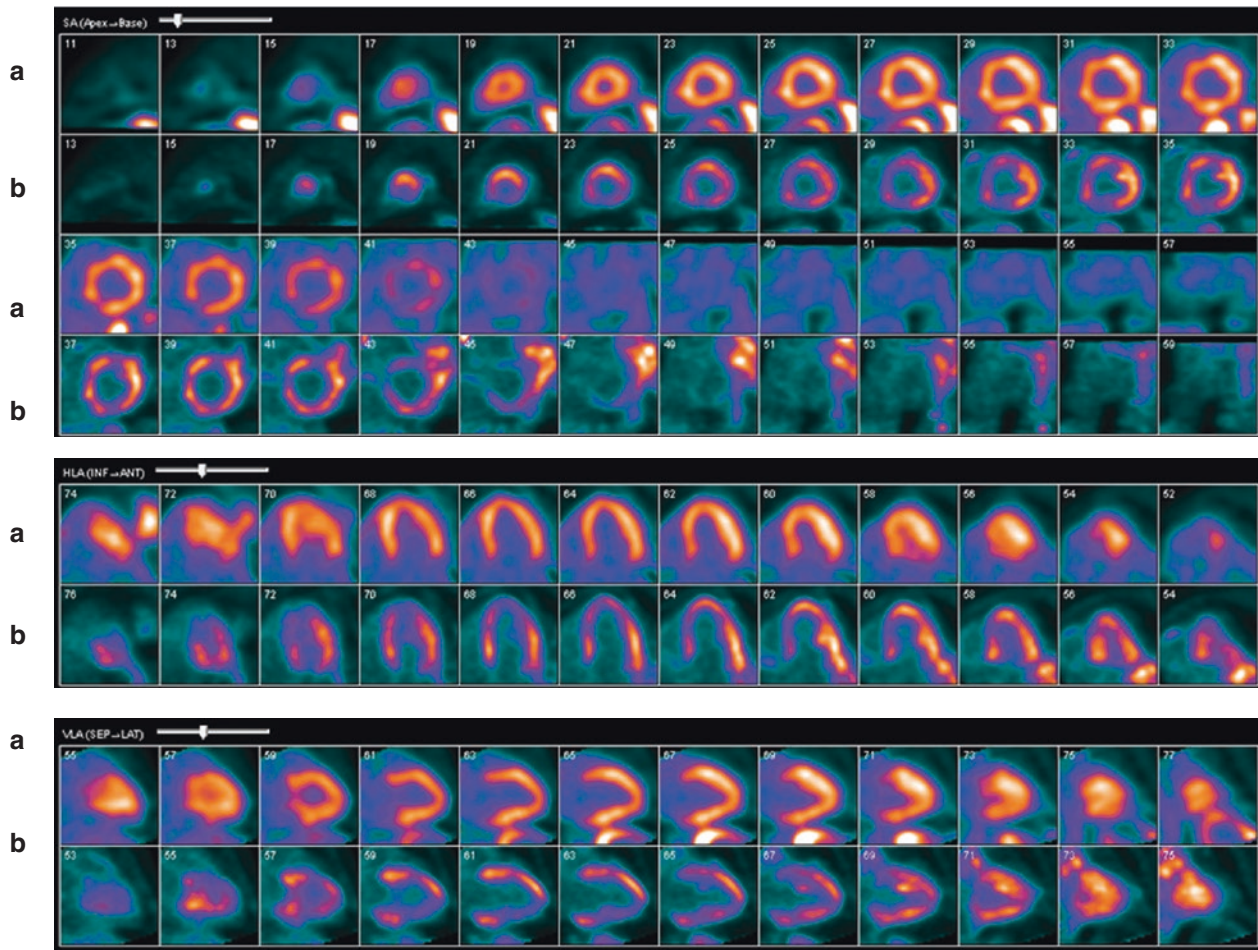
As shown in Table 13.1, the current diagnostic criteria for cardiac sarcoidosis use endomyocardial biopsy or a combination of extracardiac biopsy with typical clinical and imaging features in the heart [4]. Clinical manifestations (as listed on Table 13.1 for the Heart Rhythm Society) are typically not specific to diagnose cardiac involvement. Echocardiography is not sensitive to diagnose cardiac sarcoidosis. Cardiovascular magnetic resonance (CMR), on the other hand, provides characteristic patterns of late gadolinium enhancement that are highly sensitive for the diagnosis of cardiac sarcoidosis [5]. However, neither echocardiography nor CMR can provide the necessary information on active myocardial inflammation to guide immunosuppressive therapy [5]. Moreover, CMR is contraindicated in individuals with devices not compatible with MRI. The available clinical tools to image myocardial inflammation comprise radionuclide imaging with  $^{67}\text{Gallium-citrate}$  [6] or  $^{18}\text{F-FDG}$  [7].

Japanese Ministry of Health and Welfare
<i>Histological diagnosis</i>
Cardiac sarcoidosis confirmed by endomyocardial biopsy, and histological or clinical diagnosis of extracardiac sarcoidosis
<i>Clinical diagnosis group</i>
Histological or clinical diagnosis of extracardiac sarcoidosis <i>and</i> two or more major criteria <i>or</i> one major criterion and two or more minor criteria:
<i>Major criteria</i>
Advanced atrioventricular block
Basal thinning of the interventricular septum
$^{67}\text{Gallium}$ uptake in the heart
LVEF <50%
<i>Minor criteria</i>
Electrocardiography: Ventricular tachycardia, PVCs, RBBB, abnormal axis, abnormal Q wave
Echocardiography: Structural or wall motion abnormality
Radionuclide imaging: Perfusion defect on $^{201}\text{thallium}$ , $^{99\text{m}}\text{technetium-sestamibi-tetrofosmin}$
Cardiac MRI: late gadolinium enhancement
Endomyocardial biopsy: Moderate fibrosis or monocyte infiltration
Heart Rhythm Society
<i>Histological diagnosis from myocardial tissue</i>
Noncaseating granuloma on endomyocardial biopsy with no alternative cause identified
<i>Clinical diagnosis</i>
Probable diagnosis of cardiac sarcoidosis exists if there is histological diagnosis of extracardiac sarcoidosis <i>and</i> one or more of the following are present:
Cardiomyopathy or atrioventricular block responsive to immunosuppressive therapy
Unexplained reduced LVEF (<40%)
Unexplained ventricular tachycardia
Mobitz II second- or third-degree heart block
Patchy $^{18}\text{F-FDG}$ uptake on cardiac PET consistent with cardiac sarcoidosis
Late gadolinium enhancement on CMR consistent with cardiac sarcoidosis
Cardiac $^{67}\text{gallium}$ uptake
Exclusion of other causes of cardiac manifestations

CMR cardiac magnetic resonance imaging, LVEF left ventricular ejection fraction, PVCs premature ventricular complexes, RBBB right bundle branch block

**Table 13.1** Diagnostic criteria for cardiac sarcoidosis

Owing to its poor sensitivity,  $^{67}\text{Ga}$ -citrate SPECT imaging has been largely replaced in clinical practice by  $^{18}\text{F}$ -FDG PET/CT imaging [5].  $^{18}\text{F}$ -FDG PET/CT imaging tracks myocardial uptake of glucose, which is increased in sarcoid granulomas because of the high glycolytic activity of the inflammatory cells.  $^{18}\text{F}$ -FDG PET/CT thus provides high accuracy to diagnose cardiac sarcoidosis, using a reference standard of Japanese Ministry Criteria or endomyocardial biopsy, with a pooled sensitivity of 89% (95% CI, 79–96%) and a pooled specificity of 78% (95% CI, 68–86%) [8]. When compared with echocardiography, CMR, and  $^{67}\text{Ga}$  scintigraphy,  $^{18}\text{F}$ -FDG PET/CT is more accurate [5]. Myocardial  $^{18}\text{F}$ -FDG uptake, however, can be nonspecific; it cannot differentiate between normal myocardial glucose utilization, myocardial inflammation, ischemia, tumor, or infection. Hence, myocardial  $^{18}\text{F}$ -FDG imaging of sarcoidosis is performed with a special dietary preparation to suppress physiological glucose utilization. As myocardial uptake of  $^{18}\text{F}$ -FDG can be physiological, interpretation of diffuse myocardial FDG uptake, as well as focal uptake in the basal lateral wall, can be challenging. For this and other reasons, although  $^{18}\text{F}$ -FDG PET/CT can be very valuable for the initial evaluation of patients with suspected cardiac sarcoidosis, CMR is the preferred first test. Once a diagnosis of cardiac sarcoidosis is suspected on CMR or confirmed by endomyocardial biopsy,  $^{18}\text{F}$ -FDG imaging is often performed to assess the burden of myocardial inflammation at baseline and during followup, to assess changes in response to therapy [5, 9] (Fig. 13.2).

**$^{99m}\text{Tc}$ -sestamibi SPECT/CT rest MPI and  $^{18}\text{F}$ -FDG PET/CT**

**Fig. 13.2** Imaging in a patient with suspected cardiac sarcoidosis. A 44-year-old man with progressive dyspnea for 1 year underwent CT scan of the chest that revealed prominent hilar lymphadenopathy. Due to a concern for lymphoma, an  $^{18}\text{F}$ -FDG PET scan was performed, which revealed focal cardiac FDG uptake suggestive of cardiac sarcoidosis. A CMR confirmed late gadolinium enhancement (LGE, fibrosis) and increased T2 signal (edema) of the left and right ventricles, confirming cardiac sarcoidosis. The  $^{18}\text{F}$ -FDG scan was repeated (**a–d**) using the protocol for sarcoidosis. One day prior to the  $^{18}\text{F}$ -FDG PET/CT scan, a high-fat, low-carbohydrate diet was provided for two large meals, followed by an overnight fast. On the day of the study, rest myocardial perfusion imaging (MPI) was performed with 10 mCi of  $^{99m}\text{Tc}$ -sestamibi and gated attenuation-corrected SPECT/CT imaging (**a**). Following the perfusion scan, the patient received 8 mCi of  $^{18}\text{F}$ -FDG intravenously and cardiac (10-minute, **b**) and whole body  $^{18}\text{F}$ -FDG PET/CT images (3 minutes per

bed position eyes to kidneys; **c** and **d**) were performed 90 minutes later in a 3D mode, using a non-gated acquisition. The images showed a pattern of focal-on-diffuse myocardial uptake of  $^{18}\text{F}$ -FDG in the left ventricle. A pattern of diffuse myocardial uptake can represent physiological glucose utilization, so CMR images were reviewed. They showed regions of LGE corresponding to the regions of focal  $^{18}\text{F}$ -FDG uptake in the lateral wall (**c** and **d**), confirming that  $^{18}\text{F}$ -FDG uptake in the lateral wall was pathological. Also, extensive focal uptake was noted in the right ventricle, and in the mediastinal, hilar, and supraclavicular lymph nodes (**c** and **d**). The left ventricular ejection fraction was 64%. The patient was started on high-dose steroids (40 g PO QD, with a plan to taper) and methotrexate 15 mg orally weekly. He received an implantable cardioverter-defibrillator (ICD), which over the next 6 months revealed frequent runs of ventricular tachycardia terminated by antitachycardia pacing. CTAC–low dose CT obtained for attenuation correction

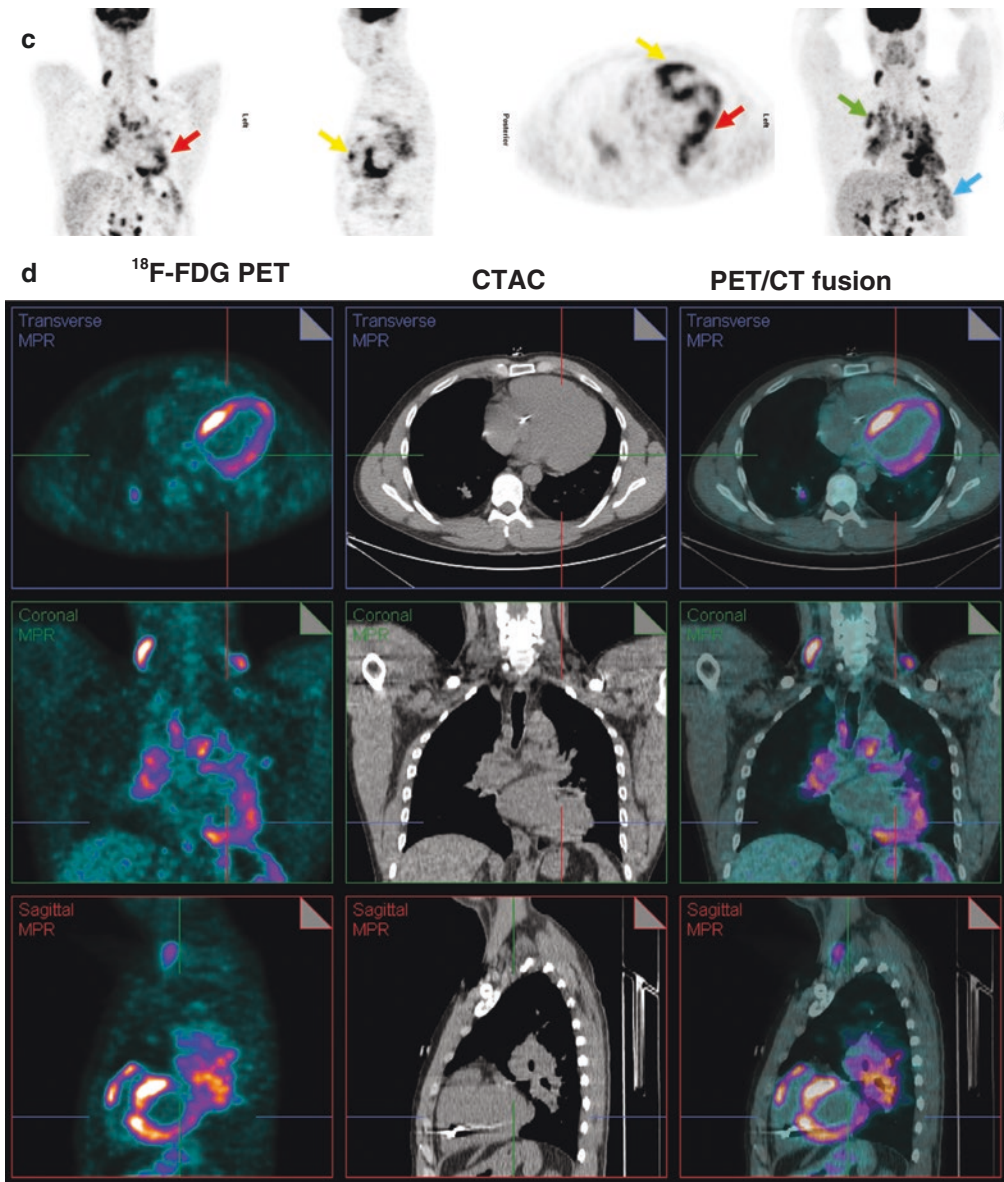


**Fig. 13.2** (continued)

A pattern of normal perfusion with focally increased  $^{18}\text{F}$ -FDG uptake, or a perfusion defect with focally increased  $^{18}\text{F}$ -FDG uptake, is characteristic of active sarcoidosis. A perfusion metabolism mismatch pattern is also a hallmark of hibernating myocardium, hence it is imperative to exclude ischemic heart disease by stress imaging or coronary angiography before diagnosing cardiac sarcoidosis in this pattern [4, 5, 10]. In the absence of myocardial  $^{18}\text{F}$ -FDG uptake, the presence of myocardial perfusion defects on attenuation-corrected images can signify scarred myocardium.

In one study, 118 patients with suspected sarcoidosis who underwent  $^{18}\text{F}$ -FDG PET/CT with myocardial perfusion imaging were followed up for a median of 1.5 years. A total of 31 adverse events (27 ventricular tachyarrhythmias and 8 deaths) were observed (Fig. 13.3). A normal myocardial perfusion and no cardiac  $^{18}\text{F}$ -FDG uptake portended the best survival free of ventricular tachyarrhythmias. If either  $^{18}\text{F}$ -FDG PET/CT or myocardial perfusion imaging was abnormal, the rate of event-free survival was worse, and if both were abnormal, that pattern conferred the highest risk.

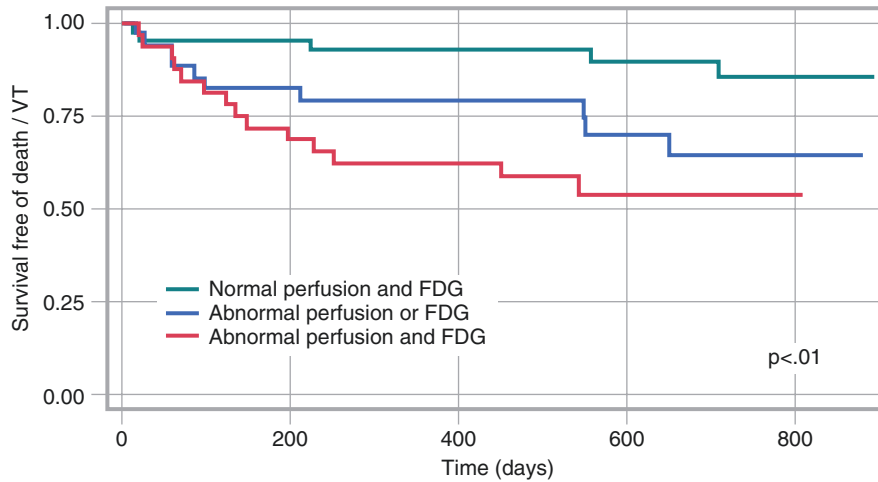


**Fig. 13.3** Prognostic value of  $^{18}\text{F}$ -FDG and myocardial perfusion imaging in cardiac sarcoidosis. (From Blankstein et al. [7]; with permission from Elsevier)

$^{18}\text{F}$ -FDG PET/CT is also used to assess response to therapy (Fig. 13.4).  $^{18}\text{F}$ -FDG imaging is performed to assess the burden of myocardial inflammation at baseline and during followup to assess changes response to therapy [5, 9].  $^{18}\text{F}$ -FDG PET/CT sarcoidosis imaging is a hot-spot imaging tracer. Hence, visual interpretation of the images can be limited in evaluating change. Myocardial radiotracer uptake is quantified for assessment of changes using standardized uptake value (SUV), volume of inflamed myocardium (using a threshold SUVmax value), or target-to-background ratio [9].

#### $^{99\text{m}}\text{Tc}$ -sestamibi SPECT/CT rest MPI and $^{18}\text{F}$ FDG PET/CT

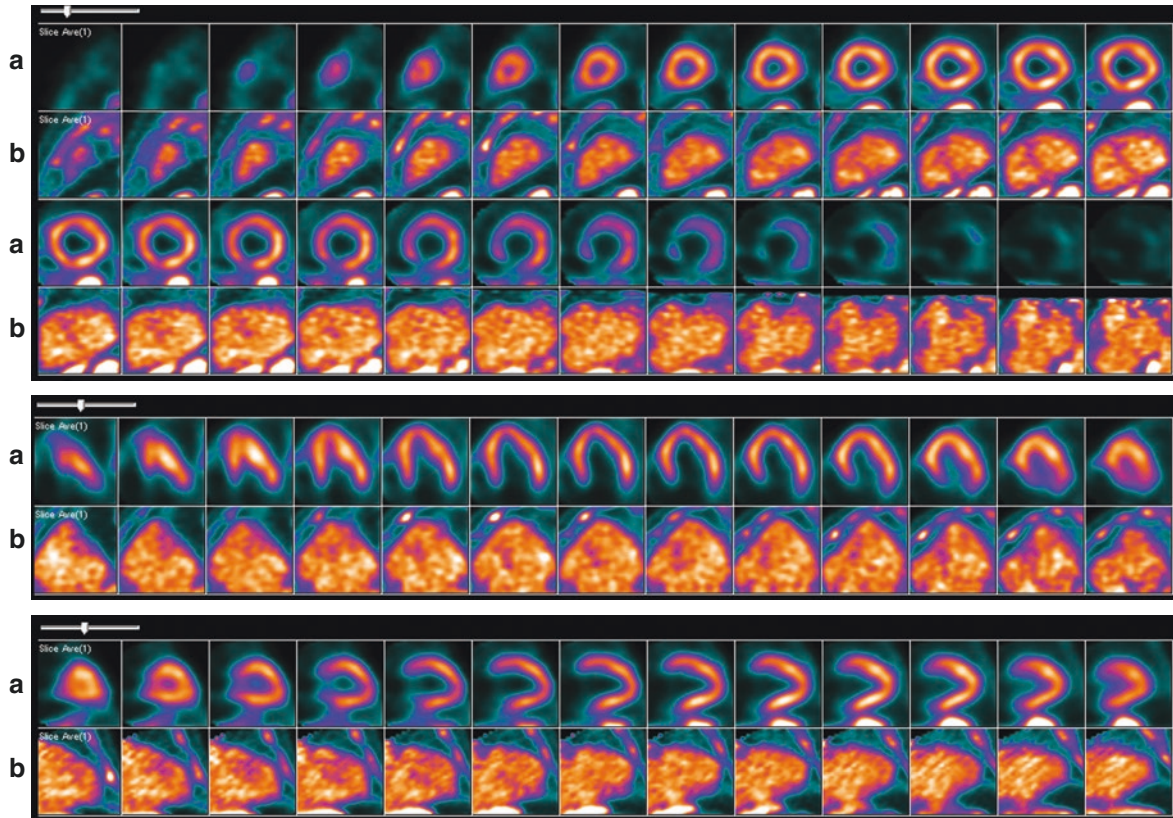


**Fig. 13.4**  $^{18}\text{F}$ -FDG PET/CT to assess response to therapy. When the patient in Fig. 13.2 returned for a follow-up  $^{18}\text{F}$ -FDG PET/CT scan 6 months later with myocardial perfusion imaging (a and b), it revealed near-complete resolution of inflammation in the heart and in the medi-

astinal nodes (c and d). Myocardial perfusion was normal (a), except for the basal inferoseptal region, which showed a small scar (best seen on the short axis images in row 3 of a). His left ventricular ejection fraction was 60%



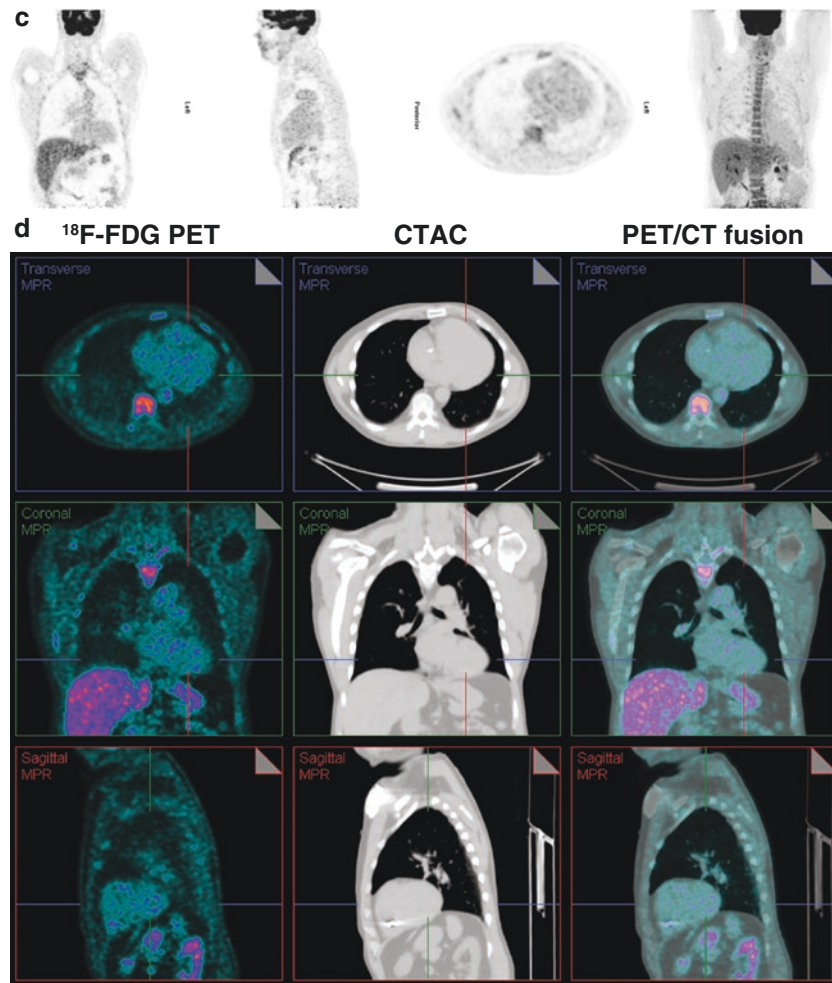


**Fig. 13.4** (continued)

Figure 13.5 outlines an approach to evaluation of cardiac sarcoidosis.

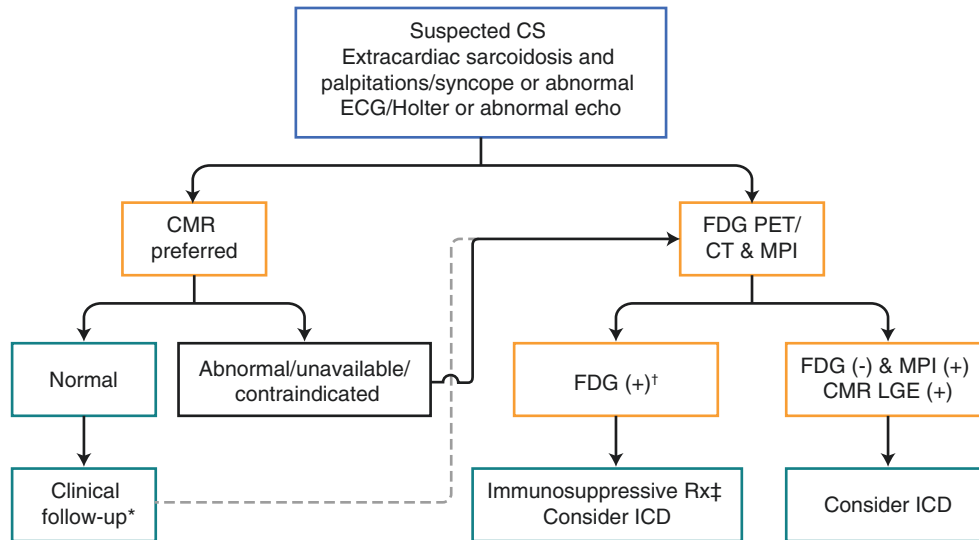


**Fig. 13.5** An approach to evaluation of cardiac sarcoidosis (CS) using  $^{18}\text{F}$ -FDG PET/CT and CMR. Patients with suspected cardiac sarcoidosis, symptoms, and imaging findings can be evaluated with either a gadolinium-enhanced CMR or  $^{18}\text{F}$ -FDG PET/CT with myocardial perfusion imaging (MPI). Imaging findings can guide immunosuppressive therapy and ICD implantation in patients with cardiac sarcoidosis. \*If

clinical suspicion is high or symptoms persist, FDG-PET/CT and MPI may be considered in patients with normal CMR; <sup>†</sup>Identify coexistent inflammation; <sup>‡</sup>Immunosuppressive therapy may be considered taking into account the amount of inflammation. (From Slart et al. [11] with permission from Springer Nature)

## Cardiovascular Prosthetic Infection

Imaging with  $^{18}\text{F}$ -FDG PET has transformed the evaluation and management of patients with infection involving cardiovascular prosthetics (Fig. 13.6) [13, 14] and devices [15, 16], including left ventricular assist devices [17].

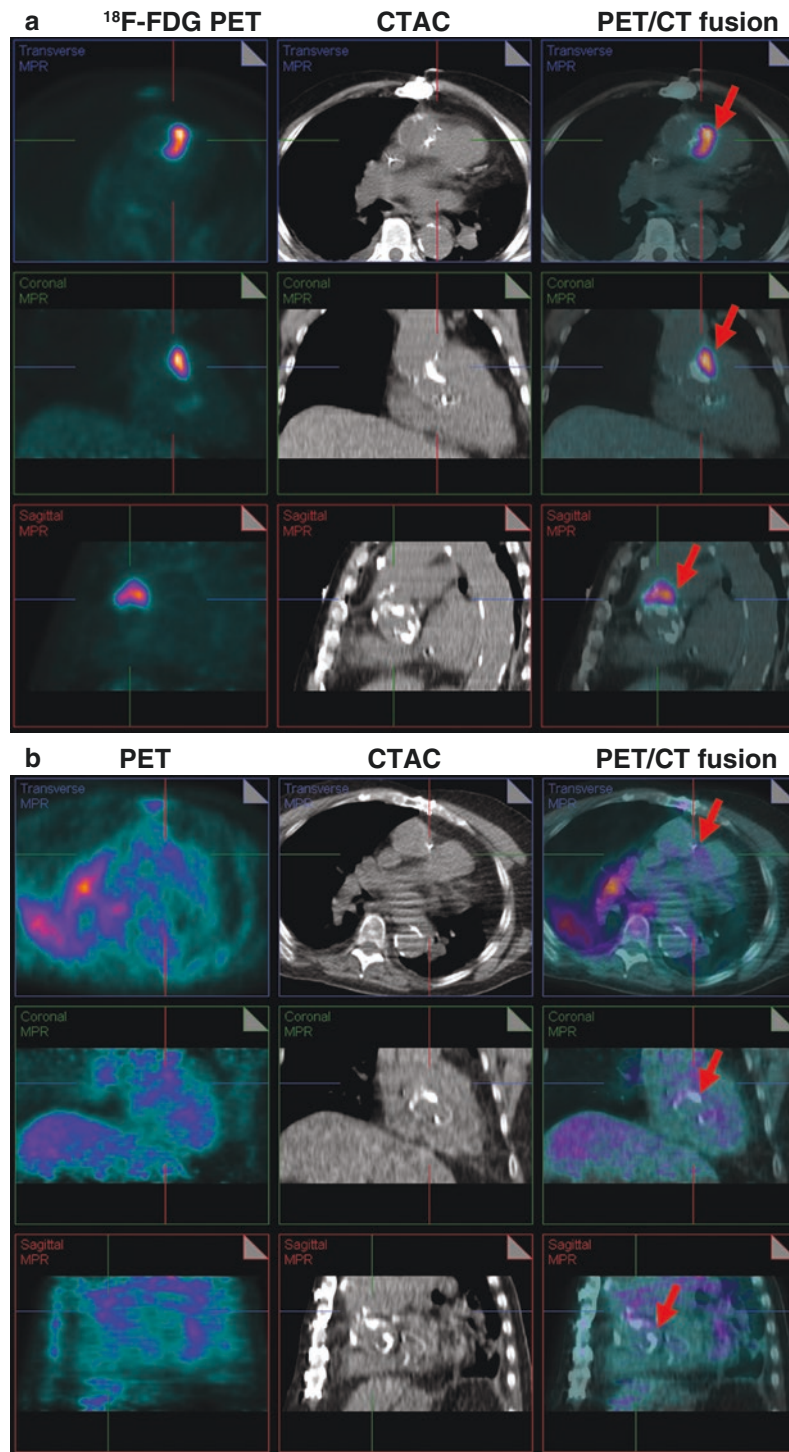


**Fig. 13.6** Utility of  $^{18}\text{F}$ -FDG PET/CT in identifying infected prosthetic material. An 88-year-old man with three prior aortic valve replacements and aortic root repair presented with fevers and blood cultures positive for *Escherichia coli*. A transesophageal echocardiogram was unrevealing. (a) Because of persistent fevers, an  $^{18}\text{F}$ -FDG PET scan was performed, which showed focal intense  $^{18}\text{F}$ -FDG uptake in the region of the ascending aorta (red arrows). The corresponding region on the non-contrast CT scan

revealed a lucency that was suspicious for a pseudoaneurysm. Iodinated contrast could not be used, owing to renal insufficiency. The patient was deemed too high-risk for a fourth aortic surgery and was managed medically. (b) The same patient was rehospitalized 18 months later with altered mental status, fevers, and a pneumonia on chest x-ray. Persistent bacteremia led to concern for recurrent endocarditis.  $^{18}\text{F}$ -FDG imaging was repeated and it revealed no uptake in the region of the aortic root

Pizzi et al. [14] showed that the addition of cardiac CT angiography with contrast to  $^{18}\text{F}$ -FDG PET improved diagnostic accuracy for the detection of infective endocarditis (Fig. 13.7).

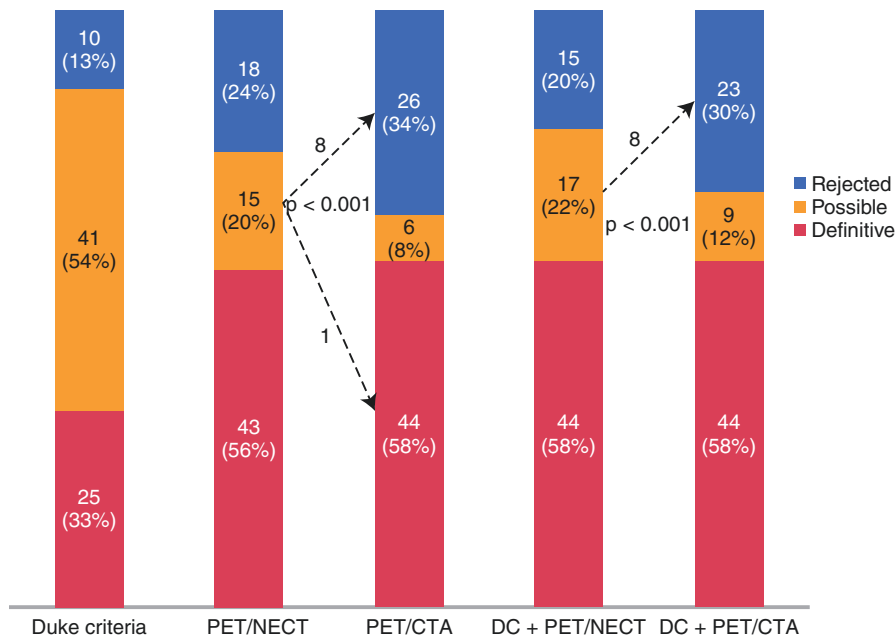
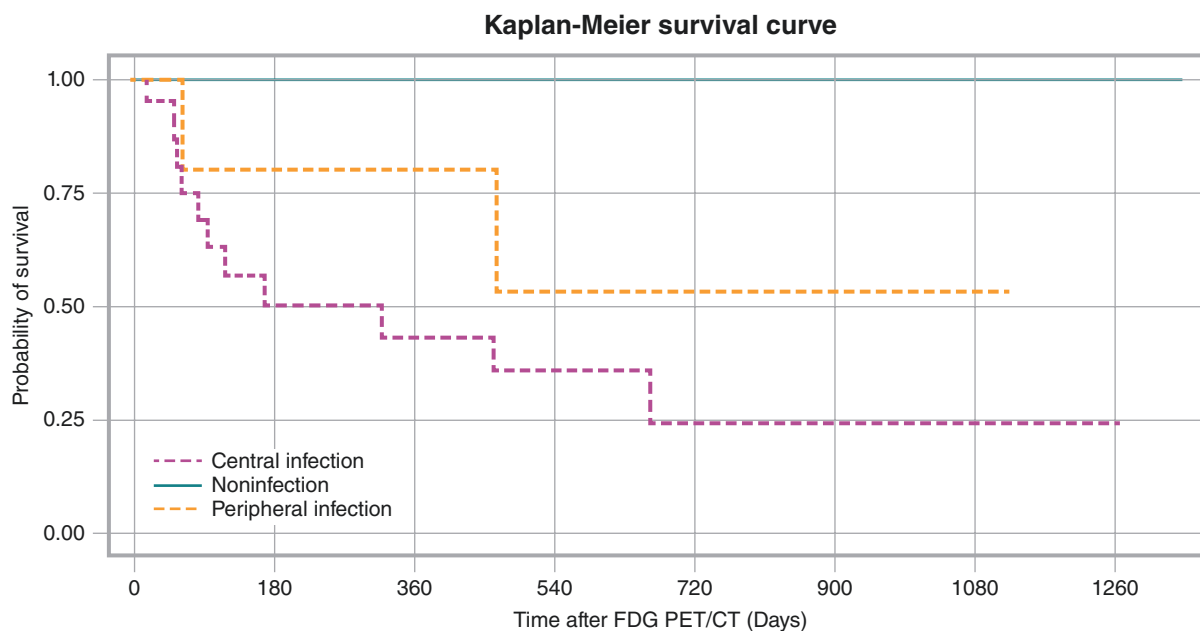


**Fig. 13.7** Incremental value of  $^{18}\text{F}$ -FDG PET/CT and contrast-enhanced cardiac CT angiography (CTA) in the diagnosis of infective endocarditis. The addition of CTA to  $^{18}\text{F}$ -FDG PET has been shown to improve diagnostic accuracy for the detection of infective endocarditis (sensitivity, specificity, positive and negative predictive values of 91%, 90.6%, 92.8%, and 88.3% for  $^{18}\text{F}$ -FDG PET/CT with CTA, versus 86.4%, 87.5%, 90.2%, and 82.9%, respectively, for  $^{18}\text{F}$ -FDG PET/CT without contrast [NECT]), and significantly improved the detection of

anatomic lesions. With the addition of CTA, the rate of infective endocarditis cases designated “possible” decreased from 20% to 8% ( $p < 0.001$ ). Duke criteria (DC) combined with  $^{18}\text{F}$ -FDG PET/CTA reclassified 47% of cases when compared with Duke criteria combined with non-contrast attenuation-correction CT, and a confirmed diagnosis of definite or rejected infective endocarditis was established in 88% of cases. (From Pizzi et al. [14]; with permission from Wolters Kluwer)

Prosthetic valve infective endocarditis is associated with high in-hospital mortality of 20–40% [18]. A multimodal imaging approach that includes echocardiography,  $^{18}\text{F}$ -FDG PET, cardiac CT, and sometimes MRI is frequently necessary in dealing with these complex diagnostic challenges. Imaging with transesophageal echocardiography remains the first-line test in most cases of suspected endocarditis [19], but echocardiography frequently may be limited in detecting endocarditis because of shadowing from the prosthetic valves and devices. Contrast-enhanced cardiac CT plays an important role in excluding epicardial CAD prior to surgery and in diagnosing valve abscess, fistula, pseudoaneurysm, and embolic phenomenon (cerebral or abdominal CT in select cases) [19]. MRI has a limited role in prosthetic valve endocarditis. It is primarily used for brain imaging to detect cerebral lesions (found in 82%), subclinical cerebral events (found in 30–40%), and clinical or subclinical cerebral embolic events (ischemic or hemorrhagic stroke, mycotic aneurysm, or abscess) [19]. Emerging literature suggests a central role for whole-body and cardiac  $^{18}\text{F}$ -FDG PET [13], and  $^{111}\text{In}$ Indium-labeled white blood cell scintigraphy [20, 21] is also accurate for the evaluation of prosthetic device infection, particularly when echocardiography is unrevealing or limited. Excellent systematic reviews and meta-analyses have summarized the utility and high diagnostic accuracy of  $^{18}\text{F}$ -FDG PET/CT for infective endocarditis [22, 23] and for cardiac implantable electronic devices (pooled sensitivity 93% and pooled specificity 98%) [16]. One of the major advantages of radionuclide scintigraphy for endocarditis is the ability to perform whole-body imaging to detect septic emboli [20].  $^{18}\text{F}$ -FDG PET/CT imaging is useful not only to diagnose infection but also to evaluate response to therapy (*see* Fig. 13.6.B) and to predict prognosis (Fig. 13.8).

Based on the emerging literature on radionuclide imaging in infective endocarditis, The European Society of Cardiology in 2015 recommended expanding to the Duke criteria to include (1) definite vegetations on echocardiography, (2) abnormal activity detected by  $^{18}\text{F}$ -FDG PET/CT (only if the prosthesis has been in place >3 months) or radiolabeled leukocyte SPECT/CT around the site of prosthetic valve implantation, and (3) a definite paravalvular lesion on cardiac CT [19].



**Number at risk**

Noninfection	7	5	4	4	3	2	2	1
Central infection	23	8	6	5	2	1	1	1
Peripheral infection	5	4	3	2	1	1	1	0

**Fig. 13.8**  $^{18}\text{F}$ -FDG for early detection and management of infections involving a left ventricular assist device (LVAD). Kim et al. [17] evaluated 35 patients with LVAD who underwent  $^{18}\text{F}$ -FDG PET/CT and found that 50% of the patients with infection died during a mean fol-

lowup of 23 months. Patients with central infection (*red line*) had much worse survival than patients with peripheral infection (*blue line*) or no infection (*green line*). (From Kim et al. [17]; with permission from Elsevier)

## Cardiac Amyloidosis

Cardiac amyloidosis is one of the most fatal forms of heart failure, with a median survival of less than 6 months for untreated AL amyloidosis [24] and about 4 years for ATTR amyloidosis [25, 26]. Amyloid fibrils are formed in the heart, most commonly from misfolded immunoglobulin light chains (produced by an abnormal plasma cell clone) or from wild-type or mutant transthyretin protein (produced by the liver). AL cardiac amyloidosis is treated very differently from ATTR cardiac amyloidosis, so identification of the type of amyloidosis is just as important as the diagnosis. Cardiac uptake of bone radiotracers has long been recognized to be increased in cardiac amyloidosis. In the early 2000s, investigators recognized that bone tracers are highly accurate for imaging the ATTR form of cardiac amyloidosis [27] but are unreliable in diagnosing the AL form [28]. This finding led to an explosion of clinical studies validating the utility of bone tracer cardiac scintigraphy to diagnose ATTR cardiac amyloidosis [27, 29], differentiate it from AL cardiac amyloidosis [30], and stratify risk in these patients [31, 32]. Cardiac scintigraphy with bone tracers is typically started 1 to 3 hours after injection of radiotracer (1 hour for  $^{99m}\text{Tc}$ -PYP and 3 hours for  $^{99m}\text{Tc}$ -DPD/HMDP); images are acquired as a planar chest study followed by a chest or cardiac SPECT study when planar imaging shows increased cardiac uptake [33]. These images are interpreted visually (positive and negative) and quantified using a visual score on the 3-hour images (Fig. 13.9) and/or a heart-to-contralateral-lung ratio on 1-hour or 3-hour planar images (Fig. 13.10) [33].

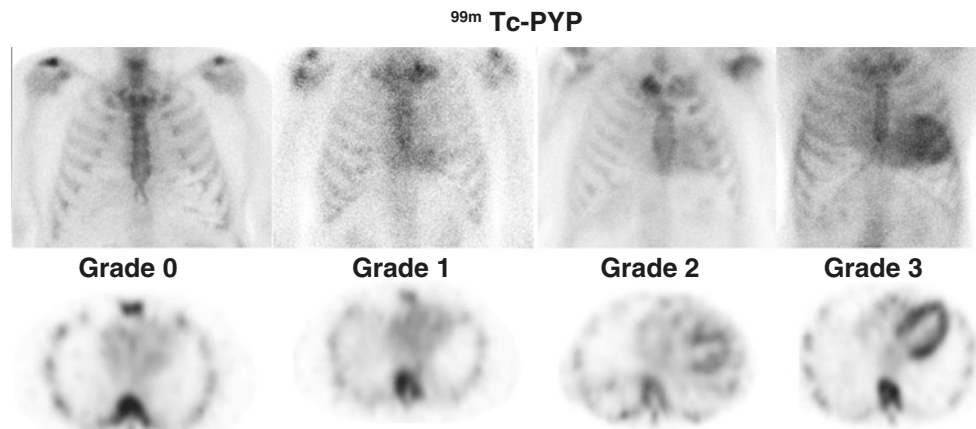


**Fig. 13.9**  $^{99m}\text{Tc}$ -pyrophosphate ( $^{99m}\text{Tc}$ -PYP) planar and SPECT chest images for the diagnosis of ATTR cardiac amyloidosis. From left to right, the images show grade 0 (no myocardial uptake), grade 1 (myocardial uptake < rib uptake), grade 2 (myocardial uptake = rib uptake)

and grade 3 (myocardial uptake > rib uptake) uptake of  $^{99m}\text{Tc}$ -PYP. Grades 2 and 3 uptake of  $^{99m}\text{Tc}$ -PYP are highly accurate in diagnosing ATTR cardiac amyloidosis in patients without a plasma cell clonal abnormality

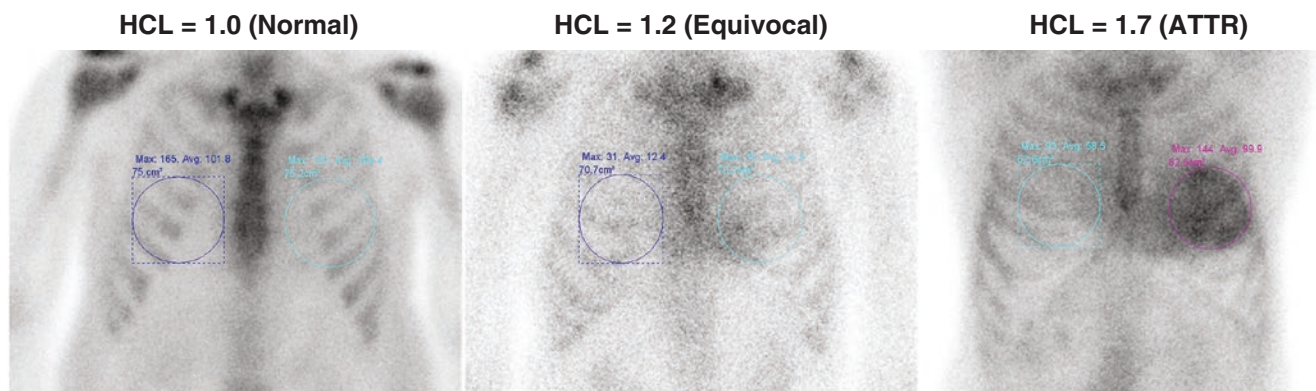


**Fig. 13.10**  $^{99m}\text{Tc}$ -PYP planar images showing the heart-to-contralateral-lung (HCL) ratio. An elliptical region of interest (ROI) is placed on the heart and mirrored on the right chest on the planar images.

A ratio greater than 1.5 of the mean counts in the ROI heart compared with the contralateral chest is highly specific in distinguishing ATTR from AL cardiac amyloidosis

In a large multicenter study, grade 2 or 3 uptake of  $^{99m}\text{Tc}$ -PYP,  $^{99m}\text{Tc}$ -DPD, or  $^{99m}\text{Tc}$ -HMDP in the context of typical symptoms and echocardiographic or CMR features demonstrated a high sensitivity (>91%) and (in the absence of a clonal abnormality) 100% specificity in diagnosing ATTR cardiac amyloidosis [34]. Heart-to-contralateral-lung ratio greater than 1.5 on 1-hour planar chest images is highly specific to distinguish AL from ATTR cardiac amyloidosis [30] and has been shown to be a marker for worse survival [31].  $^{99m}\text{Tc}$ -PYP imaging is typically performed when patients present with thick ventricles and heart failure, which are features of advanced amyloidosis, and bone tracer cardiac scintigraphy can diagnose ATTR cardiac amyloidosis early, particularly in gene-positive patients with hereditary TTR amyloidosis [35]. Bone tracer cardiac scintigraphy for amyloidosis has certain limitations, however. One small study showed that  $^{99m}\text{Tc}$ -MDP, a commonly used bone scan agent, has a lower sensitivity than  $^{99m}\text{Tc}$ -PYP to detect ATTR cardiac amyloidosis [36]. The bone tracers are also unreliable to diagnose AL cardiac amyloidosis, so if cardiac imaging shows typical features of amyloidosis and the  $^{99m}\text{Tc}$ -PYP scan is negative, patients should be evaluated for AL cardiac amyloidosis (Fig. 13.11).

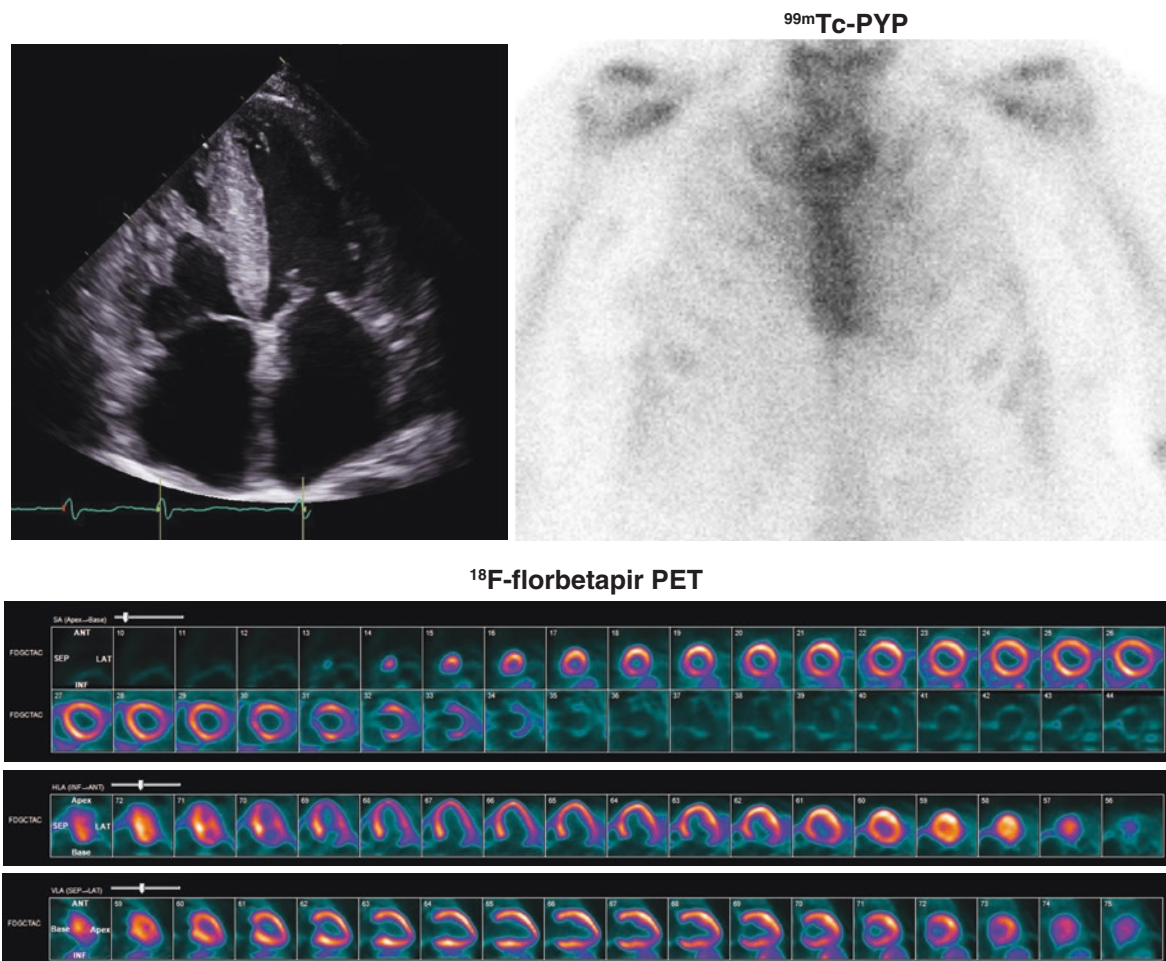


**Fig. 13.11**  $^{99m}\text{Tc}$ -PYP images in a patient with AL cardiac amyloidosis. In this 62-year-old African American man with a V122I TTR mutation, the echocardiographic (*top left panel*) and CMR imaging was consistent with cardiac amyloidosis, but the  $^{99m}\text{Tc}$ -PYP scan (*top left panel*) was negative (grade 1), excluding ATTR cardiac amyloidosis. A complete hematological evaluation (serum free light chain levels, serum

and urine immunofixation, and bone marrow biopsy) confirmed AL amyloidosis.  $^{18}\text{F}$ -florbetapir PET/CT (*bottom*) showed diffuse myocardial uptake, confirming cardiac amyloidosis. When echocardiogram and CMR are highly suggestive of cardiac amyloidosis and the  $^{99m}\text{Tc}$ -PYP scan is negative or shows grade 1 uptake, it is important to evaluate for AL cardiac amyloidosis

Amyloid-directed PET tracers, developed originally for imaging  $\beta$ -amyloid in the brain, including  $^{18}\text{F}$ -florbetapir [12, 37], florbetaben [38], and flutemetamol, can image AL cardiac amyloidosis in the heart. These clinical PET tracers are not widely available and are expensive, but they offer the advantages of imaging both AL and ATTR amyloid deposits [12, 37] (Fig. 13.12), as well as extracardiac deposits in patients with systemic AL amyloidosis [39]; they also have been shown to detect early amyloid deposits in the heart [40].

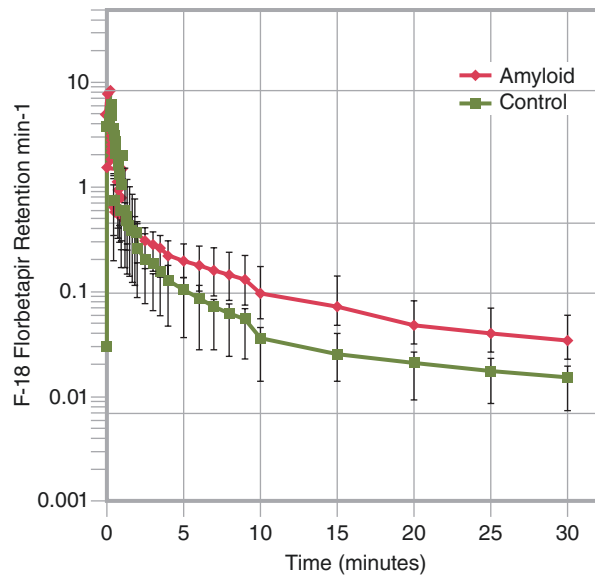


**Fig. 13.12**  $^{18}\text{F}$ -florbetapir PET/CT images and retention index in subjects with and without cardiac amyloidosis. This figure shows no myocardial  $^{18}\text{F}$ -florbetapir uptake in the control patient (*top row*) and diffuse uptake in ATTR (*middle row*) and AL (*bottom row*) cardiac amyloido-

sis. The graph on the right shows that the  $^{18}\text{F}$ -florbetapir myocardial retention index is significantly higher in the amyloid group (*red line*) than in the non-amyloid control group (*green line*)



Figure 13.13 presents a proposed approach to the evaluation of cardiac ATTR amyloidosis using bone tracer scintigraphy [34].

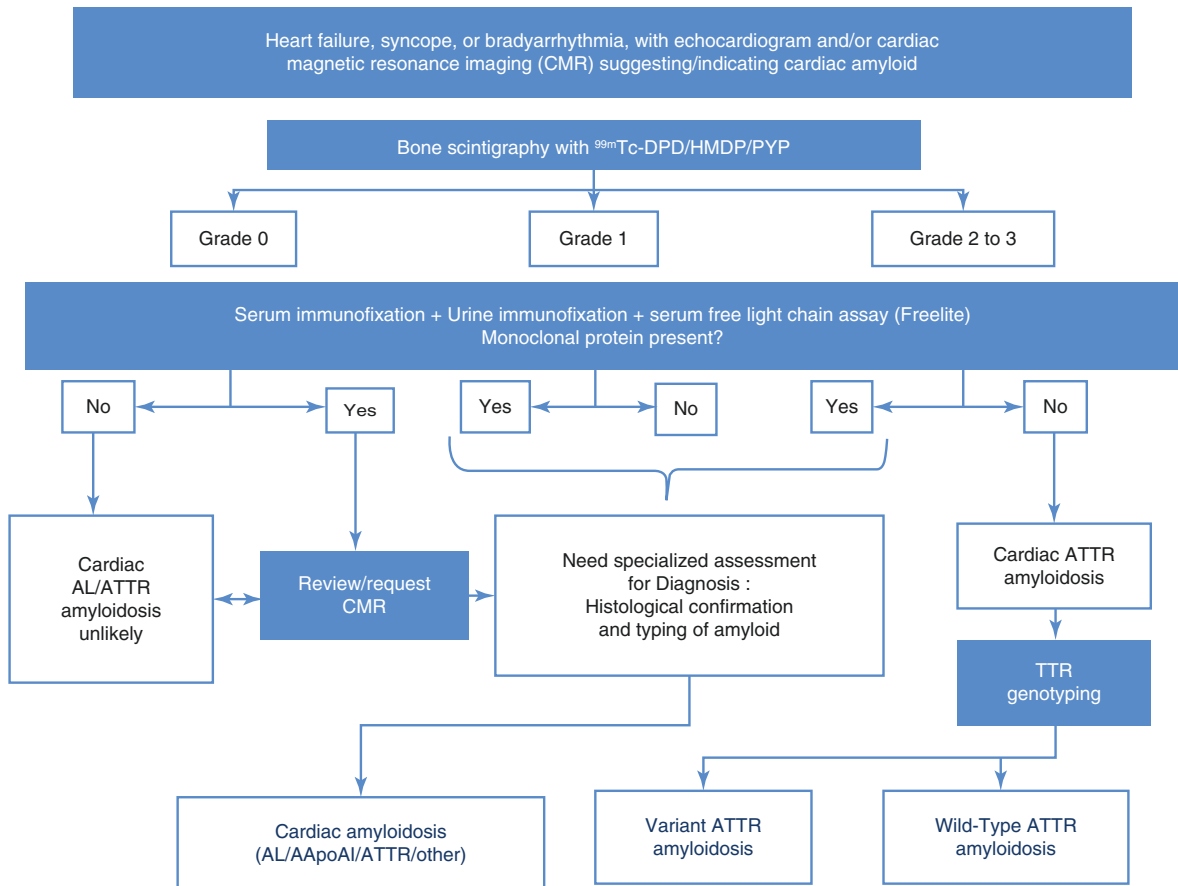


**Fig. 13.13** A proposed approach to evaluation of cardiac ATTR amyloidosis using bone tracer scintigraphy. A grade 2 or 3  $^{99m}\text{Tc}$ -PYP myocardial uptake in the absence of evidence of plasma cell dyscrasia is nearly 100% specific for a diagnosis of ATTR cardiac amyloidosis.

Endomyocardial biopsy may be considered when the  $^{99m}\text{Tc}$ -PYP results are equivocal and the diagnosis is not clear after imaging-based evaluation. (From Gillmore et al. [34]; with permission from Wolters Kluwer)

**Conflicts of Interest** RHF has received consulting fees from Ionis Pharmaceuticals and Alnylam Pharmaceuticals and research funding from GlaxoSmithKline. SD has received consulting fees from Pfizer, AAA, and GE Healthcare.

**Funding Support** SD and RHF are supported by NIH RO1 grant (RO1 HL 130563 and RO1 HL 150342); SD is supported by American Heart Association Grant (AHA 16 CSA 2888 0004, and AHA19SRG34950011).

## References

- Perry A, Vuitch F. Causes of death in patients with sarcoidosis. A morphologic study of 38 autopsies with clinicopathologic correlations. *Arch Pathol Lab Med.* 1995;119:167–72.
- Iannuzzi MC, Rybicki BA, Teirstein AS. Sarcoidosis. *N Engl J Med.* 2007;357:2153–65.
- Dorbala S, Shaw LJ. Molecular phenotyping of infiltrative cardiomyopathies: the future. *J Nucl Cardiol.* 2019;26:154–7.
- Chareonthitawee P, Beanlands RS, Chen W, Dorbala S, Miller EJ, Murthy VL, et al. Joint SNMMI-ASNC expert consensus document on the role of (18)F-FDG PET/CT in cardiac sarcoid detection and therapy monitoring. *J Nucl Cardiol.* 2017;24:1741–58.
- Slart R, Glaudemans A, Lancellotti P, Hyafil F, Blankstein R, Schwartz RG, et al. A joint procedural position statement on imaging in cardiac sarcoidosis: from the Cardiovascular and Inflammation & Infection Committees of the European Association of Nuclear Medicine, the European Association of Cardiovascular Imaging, and the American Society of Nuclear Cardiology. *J Nucl Cardiol.* 2018;25:298–319.
- Okayama K, Kurata C, Tawarahara K, Wakabayashi Y, Chida K, Sato A. Diagnostic and prognostic value of myocardial scintigraphy with thallium-201 and gallium-67 in cardiac sarcoidosis. *Chest.* 1995;107:330–4.
- Blankstein R, Osborne M, Naya M, Waller A, Kim CK, Murthy VL, et al. Cardiac positron emission tomography enhances prognostic assessments of patients with suspected cardiac sarcoidosis. *J Am Coll Cardiol.* 2014;63:329–36.
- Youssef G, Leung E, Mylonas I, Nery P, Williams K, Wisenberg G, et al. The use of 18F-FDG PET in the diagnosis of cardiac sarcoidosis: a systematic review and metaanalysis including the Ontario experience. *J Nucl Med.* 2012;53:241–8.
- Waller AH, Blankstein R. Quantifying myocardial inflammation using F18-fluorodeoxyglucose positron emission tomography in cardiac sarcoidosis. *J Nucl Cardiol.* 2014;21:940–3.
- Dilsizian V, Bacharach SL, Beanlands RS, Bergmann SR, Delbeke D, Dorbala S, et al. ASNC imaging guidelines/SNMMI procedure standard for positron emission tomography (PET) nuclear cardiology procedures. *J Nucl Cardiol.* 2016;23:1187–226.
- Slart R, Glaudemans A, Lancellotti P, Hyafil F, Blankstein R, Schwartz RG, Jaber WA, Russell R, Gimelli A, Rouzet F, Hacker M, Gheysens O, Plein S, Miller EJ, Dorbala S, Donal E and Document Reading G. A joint procedural position statement on imaging in cardiac sarcoidosis: from the Cardiovascular and Inflammation & Infection Committees of the European Association of Nuclear Medicine, the European Association of Cardiovascular Imaging, and the American Society of Nuclear Cardiology. *Journal of nuclear cardiology : official publication of the American Society of Nuclear Cardiology.* 2018;25:298–319.
- Dorbala S, Vangala D, Semer J, Strader C, Bruyere JR, Di Carli MF, et al. Imaging cardiac amyloidosis: a pilot study using 18F-florbetapir positron emission tomography. *Eur J Nucl Med Mol Imaging.* 2014;41:1652–62.
- Saby L, Laas O, Habib G, Cammilleri S, Mancini J, Tessonnier L, et al. Positron emission tomography/computed tomography for diagnosis of prosthetic valve endocarditis: increased valvular 18F-fluorodeoxyglucose uptake as a novel major criterion. *J Am Coll Cardiol.* 2013;61:2374–82.
- Pizzi MN, Roque A, Fernandez-Hidalgo N, Cuellar-Calabria H, Ferreira-Gonzalez I, Gonzalez-Alujas MT, et al. Improving the diagnosis of infective endocarditis in prosthetic valves and intracardiac devices with 18F-fluorodeoxyglucose positron emission tomography/computed tomography angiography: initial results at an infective endocarditis referral center. *Circulation.* 2015;132:1113–26.
- Sarrazin JF, Philippon F, Tessier M, Guimond J, Molin F, Champagne J, et al. Usefulness of fluorine-18 positron emission tomography/computed tomography for identification of cardiovascular implantable electronic device infections. *J Am Coll Cardiol.* 2012;59:1616–25.
- Juneau D, Golfam M, Hazra S, Zuckier LS, Garas S, Redpath C, et al. Positron emission tomography and single-photon emission computed tomography imaging in the diagnosis of cardiac implantable electronic device infection: a systematic review and meta-analysis. *Circ Cardiovasc Imaging.* 2017;10. pii: e005772.
- Kim J, Feller ED, Chen W, Liang Y, Dilsizian V. FDG PET/CT for early detection and localization of left ventricular assist device infection: impact on patient management and outcome. *JACC Cardiovasc Imaging.* 2019;12:722–9.
- Halani T, Chu VH, Park LP, Cecchi E, Corey GR, Durante-Mangoni E, et al. In-hospital and 1-year mortality in patients undergoing early surgery for prosthetic valve endocarditis. *JAMA Intern Med.* 2013;173:1495–504.
- Habib G, Lancellotti P, Antunes MJ, Bongiorni MG, Casalta JP, Del Zotti F, et al. 2015 ESC guidelines for the management of infective endocarditis: The Task Force for the Management of Infective Endocarditis of the European Society of Cardiology (ESC). Endorsed by: European Association for Cardio-Thoracic Surgery (EACTS), the European Association of Nuclear Medicine (EANM). *Eur Heart J.* 2015;36:3075–128.
- Erba PA, Conti U, Lazzeri E, Sollini M, Doria R, De Tommasi SM, et al. Added value of 99mTc-HMPAO-labeled leukocyte SPECT/CT in the characterization and management of patients with infectious endocarditis. *J Nucl Med.* 2012;53:1235–43.
- Erba PA, Sollini M, Conti U, Bandera F, Tascini C, De Tommasi SM, et al. Radiolabeled WBC scintigraphy in the diagnostic workup of patients with suspected device-related infections. *JACC Cardiovasc Imaging.* 2013;6:1075–86.
- Gomes A, Glaudemans A, Touw DJ, van Melle JP, Willems TP, Maass AH, et al. Diagnostic value of imaging in infective endocarditis: a systematic review. *Lancet Infect Dis.* 2017;17:e1–14.
- Mahmood M, Kendi AT, Ajmal S, Farid S, O'Horo JC, Chareonthitawee P, et al. Meta-analysis of 18F-FDG PET/CT in the diagnosis of infective endocarditis. *J Nucl Cardiol.* 2019;26:922–35.
- Kyle RA, Gertz MA. Primary systemic amyloidosis: clinical and laboratory features in 474 cases. *Semin Hematol.* 1995;32:45–59.
- Connors LH, Doros G, Sam F, Badiee A, Seldin DC, Skinner M. Clinical features and survival in senile systemic amyloidosis: comparison to familial transthyretin cardiomyopathy. *Amyloid.* 2011;18 Suppl 1:157–9.
- Dungu JN, Valencia O, Pinney JH, Gibbs SD, Rowczenio D, Gilbertson JA, et al. CMR-based differentiation of AL and ATTR cardiac amyloidosis. *JACC Cardiovasc Imaging.* 2014;7:133–42.
- Perugini E, Guidalotti PL, Salvi F, Cooke RM, Pettinato C, Riva L, et al. Noninvasive etiologic diagnosis of cardiac amyloidosis using 99mTc-3,3-diphosphono-1,2-propanodicarboxylic acid scintigraphy. *J Am Coll Cardiol.* 2005;46:1076–84.

28. Gertz MA, Brown ML, Hauser MF, Kyle RA. Utility of technetium Tc 99m pyrophosphate bone scanning in cardiac amyloidosis. *Arch Intern Med.* 1987;147:1039–44.
29. Rapezzi C, Guidalotti P, Salvi F, Riva L, Perugini E. Usefulness of 99mTc-DPD scintigraphy in cardiac amyloidosis. *J Am Coll Cardiol.* 2008;51:1509–10; author reply 1510.
30. Bokhari S, Castaño A, Pozniakoff T, Deslisle S, Latif F, Maurer MS. 99mTc-pyrophosphate scintigraphy for differentiating light-chain cardiac amyloidosis from the transthyretin-related familial and senile cardiac amyloidoses. *Circ Cardiovasc Imaging.* 2013;6:195–201.
31. Castaño A, Haq M, Narotsky DL, Goldsmith J, Weinberg RL, Morgenstern R, et al. Multicenter study of planar technetium 99m pyrophosphate cardiac imaging: predicting survival for patients with ATTR cardiac amyloidosis. *JAMA Cardiol.* 2016;1:880–9.
32. Rapezzi C, Quarta CC, Guidalotti PL, Pettinato C, Fanti S, Leone O, et al. Role of 99mTc-DPD scintigraphy in diagnosis and prognosis of hereditary transthyretin-related cardiac amyloidosis. *JACC Cardiovasc Imaging.* 2011;4:659–70.
33. Dorbala S, Bokhari S, Miller E, Bullock-Palmer R, Soman P, Thompson R. 99mTechnetium-Pyrophosphate imaging for transthyretin cardiac amyloidosis. ASNC Practice Points. American Society of Nuclear Cardiology, Fairfax, VA. 2016. <https://www.asnc.org/Files/Practice%20Resources/Practice%20Points/ASNC%20Practice%20Point-99mTechnetiumPyrophosphateImaging2016.pdf>. Accessed 26 Aug 2019.
34. Gillmore JD, Maurer MS, Falk RH, Merlini G, Damy T, Dispenzieri A, et al. Nonbiopsy diagnosis of cardiac transthyretin amyloidosis. *Circulation.* 2016;133:2404–12.
35. Haq M, Pawar S, Berk JL, Miller EJ, Ruberg FL. Can (99m) Tc-Pyrophosphate aid in early detection of cardiac involvement in asymptomatic variant TTR amyloidosis? *JACC Cardiovasc Imaging.* 2017;10:713–4.
36. Lee VW, Caldarone AG, Falk RH, Rubinow A, Cohen AS. Amyloidosis of heart and liver: comparison of Tc-99m pyrophosphate and Tc-99m methylene diphosphonate for detection. *Radiology.* 1983;148:239–42.
37. Park MA, Padera RF, Belanger A, Dubey S, Hwang DH, Veeranna V, et al. 18F-Florbetapir binds specifically to myocardial light chain and transthyretin amyloid deposits: autoradiography study. *Circ Cardiovasc Imaging.* 2015;8. pii:e002954.
38. Law WP, Wang WY, Moore PT, Mollee PN, Ng AC. Cardiac amyloid imaging with 18F-florbetaben positron emission tomography: a pilot study. *J Nucl Med.* 2016;57:1733–9.
39. Wagner T, Page J, Burniston M, Skillen A, Ross JC, Manwani R, et al. Extracardiac (18)F-florbetapir imaging in patients with systemic amyloidosis: more than hearts and minds. *Eur J Nucl Med Mol Imaging.* 2018;45:1129–38.
40. Cuddy SAM, Bravo PE, Falk RH, El-Sady S, Kijewski MF, Park MA, Ruberg FL, Sancharawala V, Landau H, Yee AJ, Bianchi G, Di Carli MF, Cheng SC, Jerosch-Herold M, Kwong RY, Liao R and Dorbala S. Improved Quantification of Cardiac Amyloid Burden in Systemic Light Chain Amyloidosis: Redefining Early Disease? *JACC Cardiovascular imaging.* 2020;13:1325–1336